STUDY OF CALCITE PRECIPITATION IN WELL CONDITIONS USING THE DDPM-DEM APPROACH

S.F.R. DA CRUZ†, F.A.R. PEREIRA†, D.C. RIBEIRO†, A.L. MARTINS[4] and O.J. ROMERO†

† *Graduate Program in Energy, Federal University of Espirito Santo – UFES, São Mateus, ES, Brazil*
‡ *Petrobras Research and Development Center – CENPES, Rio de Janeiro, RJ, Brazil*
suellenfrigatto@gmail.com; fabio.a.pereira@ufes.br; daniel.ribeiro@ufes.br; aleibsohn@petrobras.com.br; oldrich.romero@ufes.

***Abstract*— The extraction of oil results in scaling problems in various stages of the production process. The scale reduces the flow cross-sectional area, increasing pressure drop and reducing oil production. In this work, a three-dimensional, transient, turbulent, biphasic flow is modeled by combining of the Dense Discrete Phase Model (DDPM) and Discrete Element Method (DEM). The authors analyze the influence of certain parameters on particle deposition, which represents the calcium carbonate-scaling formation, on the internal wall of a horizontal pipeline in well conditions. The obtained results show that the particle deposition is higher at lower Reynolds numbers. The results also show that the use of DEM model is more representative, but due to high computational effort required, it application in complex geometries will be carefully evaluated.**

***Keywords*— Flow assurance, particle deposition, carbonate scaling, DDPM, DEM..**

I. INTRODUCTION

The oil extraction, especially in the case of typical presalt carbonate reservoirs, results in the formation of carbonate scaling in the various stages of the production process. Mitigating this problem is important in the petroleum industry to reduce costs and better use of the oil commodity (Cosmo *et al*., 2019).

Carbonate scaling, partially or wholly reduces the flow area in porous media, tubing, equipment and pipelines, as shown in Figs. 1 and 2. As a result, the pressure drop increases and oil flow rate reduces.

As mentioned by Cosmo *et al*. (2019) calcium carbonate ($CaCO_3$) is an inorganic salt that can be formed from the loss of CO_2, resulting mainly from the system's depressurization process of aqueous solution saturated with carbonate and calcium ions. The main steps are shown in Fig. 1, which is a simplified view of extremely complex flow. Initially, small solid particles are formed, a process called nucleation, which clumps neatly into a mineral from a process known as growth and agglomeration of the solid. Depending on the ordering of the particles formed, $CaCO_3$ minerals are given different names, such as calcite, aragonite and vaterite (Cosmo *et al*., 2019). Calcite is a common and most stable form of $CaCO_3$ (Cowan and Weintritt, 1976; Al Nasser *et al*., 2008).

After the agglomeration process, the particles tend to deposit and there is an encrustation process (scaling), also known as adhesion.

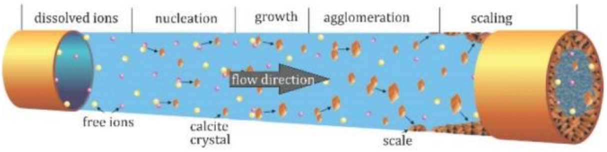

Figure 1. Main phenomena present in the process of calcite encrustation in a pipeline (Source: Cosmo *et al*., 2019).

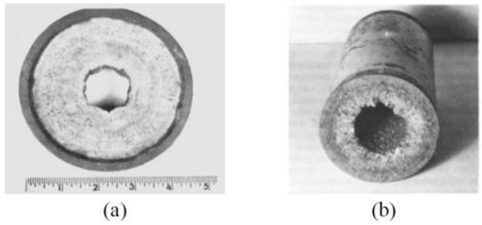

Figure 2. (a) almost pure calcium carbonate scaling, and (b) calcium carbonate and sulfate scaling ($CaCO_3$ and $CaSO_4$). (Source: Cowan and Weintritt, 1976).

Vazirian *et al*. (2016) classified the scaling process in two stages: (i) deposition, which refers to the process of heterogeneous nucleation and growth in surface roughness, and (ii) adhesion, which refers to the adherence of preexisting crystals, which nuclearize in the total solution, and accumulate as a layer on the surface.

According to Cosmo *et al*. (2019), inorganic scaling occurs as pure deposits, Fig. 2a, or as an agglomeration of different compounds, Fig. 2b.

Calcium carbonate scaling is the most common and widespread among all types of scaling, having great industrial importance. In the oil and gas production, they represent a significant problem and is one of the most studied (Cowan and Weintritt, 1976; Al Nasser *et al*., 2008; Ojaniemi *et al*., 2012).

The deep and ultra-deep oil reservoirs present in the exploratory frontiers of Brazil are mostly carbonate. Therefore, they present favorable conditions for depositing carbonate salts, especially calcite, which is, as commented, the potentially most harmful mineral (Cosmo *et al.*, 2019).

In this scenario, this study aims to numerically analyze the influence of certain parameters on the calcite precipitation process in well conditions.

II. METHODOLOGY

A. Problem specification

This paper studies the movement of spherical particles (discrete phase) conveyed by water (continuous phase) in a horizontal pipe of length $L = 10$ m and diameter $D = 0.127$ m, as shown schematically in Fig. 3.

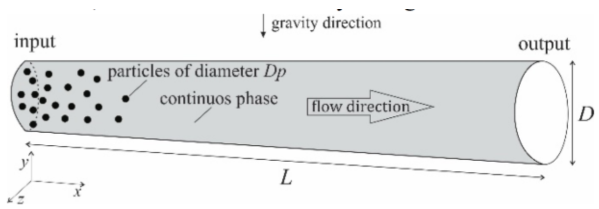

Figure 3. Schematic representation of the horizontal pipe where the calcite precipitation process occurs.

Table 1. Cases considered.

Case	Velocity V_f, m/s	Re
1	1	126,771
2	5	633,857

Particles with 750×10^{-6} m diameter (D_p) and density (ρ_P) of 2,800 kg/m^3 are injected from the left side of the pipe at a mass flow rate ($\dot{m}_p$) of 0.002 kg/s (approximately 64.7 thousand particles injected during 20 seconds of flow), and are carried by the continuous phase, which have the average velocity V_f in the input plane (asdefined in Table 1). The particles represent calcium carbonate, whose deposition in the pipe is of interest for this study. The continuous phase is water with density (ρ_f) of 998.2 kg/m^3 and viscosity (μ_f) of 0.001 kg/(m s).

The continuous phase average velocity values (V_f) of the two cases are shown in Table 1, with the Reynolds number (Re) obtained from Eq. 1.

$$Re = \frac{\rho_f V_f D}{\mu_f} \tag{1}$$

An Euler-Lagrange approach, given by the combination of the Dense Discrete Phase Model – DDPM (Popoff and Braun, 2007) with the Discrete Element Method – DEM (Cundall and Strack, 1979), was used to describe the three-dimensional behavior of the particles as detailed in the following sections of this work.

B. Dimensionless parameters

Reynolds Number:

The turbulent flow regime is determined based on the Reynolds number for a characteristic length (which in the case of a flow in a circular pipe the characteristic length is the inside diameter D), for a fluid with density ρ_f, viscosity μ_f and flowing at an average velocity V_f. Equation 1 shows this relationship and Table 1 its values.

Volumetric fraction:

The volume fraction of phase α, ε_α, is defined by the volume occupied by phase α, V_α, in relation to the local volume of the mixture V_m. The volumetric fractions of continuous fluid ($\alpha = f$) and dispersed particles ($\alpha = p$) phases are

$$\varepsilon_f = \frac{V_f}{V_f + V_p}, \tag{2}$$

$$\varepsilon_p = \frac{V_p}{V_f + V_p}, \tag{3}$$

The sum of both volumetric fractions in a given local volume is equal to the unit, according to Eq. 4.

$$\varepsilon_f + \varepsilon_p = 1, \tag{4}$$

For turbulent liquid–particle flow, when the average particle volume fraction is equal to, or greater than, 20% is considered high particle concentration flow (Hadinoto and Chew, 2010). In a high particle concentration flow, the influence of the fluid-phase turbulence on the particle fluctuating motion is insignificant as a result of the dominant role of the interparticle frictional forces in governing the particle motion (Hrenya and Sinclair, 1997).

Stokes number:

The Stokes number (S_t) is an important parameter in fluid-particle flows and is defined by the relationship between the particle response time t_p and the characteristic fluid response time t_f, as shown in Eqs. 5, 6 and 7 (Crowe *et al*., 2011).

$$S_t = \frac{t_p}{t_f}, \tag{5}$$

$$t_p = \frac{\rho_p D_p^2}{18\mu_f}, \tag{6}$$

$$t_f = \frac{D}{V_f}, \tag{7}$$

where μ_f is the dynamic fluid viscosity, D is the diameter of the domain and V_f is the average velocity of the fluid.

Gondret *et al.* (2002) investigated experimentally the bouncing motion of solid spheres onto a solid plate in an ambient fluid, and the number that characterizes the immersed collision regimes is the Stokes number. For low Stokes number, below the critical value $St_c \approx 10$, all the particle energy is dissipated in the fluid during the collision process. The particles do not modify the flow field. In this regime, no rebound is observed and the coefficient of restitution is zero. For larger Stokes number, $St > St_c$, the coefficient of restitution depends on the Stokes number, and the response of the particle related to the change in the flow field is slow, which makes the particle motion independent of fluid interaction (Chen and Chung, 1995; Crowe *et al*., 2011). Gondret *et al.* (2002) also show that the value of the critical Stokes number St_c seems to be constant, independent of the elastic properties of the solid spheres.

C. Mathematical formulation

The three-dimensional problem addressed here refers to a two-phase solid-liquid flow in transient, isothermal and turbulent conditions. The incompressible Newtonian fluid flow in horizontal pipeline (Fig. 3) is affected by the gravitational field.

Since $\boldsymbol{u}_f$ is the velocity vector, p_f the pressure, ρ_f density and ε_f volumetric fraction, the equations that govern the flow of the continuous phase f with DDPM model, proposed by Popoff and Braun (2007), are expressed by Eqs. 8 and 9.

$$\frac{\partial(\varepsilon_f \rho_f)}{\partial t} + \nabla \cdot \left(\varepsilon_f \rho_f \boldsymbol{u}_f\right) = 0, \tag{8}$$

$$\frac{\partial(\varepsilon_f \rho_f \boldsymbol{u}_f)}{\partial t} + \nabla \cdot \left(\varepsilon_f \rho_f u_f \boldsymbol{u}_f\right) = -\varepsilon_f \nabla p_f + \nabla \cdot \left(\mu_f \varepsilon_f \nabla \cdot \boldsymbol{u}_f\right) + \rho_f \varepsilon_f \boldsymbol{g} + \boldsymbol{F}_{DDPM}, \tag{9}$$

where t is time, $\boldsymbol{g}$ is the gravitational force vector and $\boldsymbol{F}_{DDPM}$ is the coupling force between the phases, expressed by Eq. 10.

$$\boldsymbol{F}_{DDPM} = \sum_{particles} \left(K_{pf}\left(\boldsymbol{u}_p - \boldsymbol{u}_f\right) + \boldsymbol{F}_{\Sigma pf}\right) \dot{m}_p \Delta t \tag{10}$$

where Δt is the time step and K_{pf} is the coupling coefficient of drag force and other forces of discrete phase,

$\boldsymbol{F}_{\Sigma pf}$, incorporated in the DDPM, which have coupling with the fluid. The coupling coefficient K_{pf} is represented by Eq. 11

$$K_{pf} = \frac{\varepsilon_p \rho_p \lambda}{t_p} \tag{11}$$

where λ is a function based on the drag coefficient C_d and the particle Reynolds number Re_p as follows $\lambda = \frac{C_d Re_p}{24}$ (Ansys, 2013).

Turbulent effects are incorporated by the $\kappa - \epsilon$ model, which solves two transport equations, one for the turbulent kinetic energy, κ, and one for the turbulence dissipation rate, ϵ, Eqs. 12 and 13, respectively.

$$\frac{\partial}{\partial t}(\rho_f \kappa) + \frac{\partial}{\partial x_j}(\rho_f \kappa \boldsymbol{u}_f) = \frac{\partial}{\partial x_j}\left[\left(\mu_f + \frac{\mu_t}{\sigma_\kappa}\right)\frac{\partial \kappa}{\partial x_j}\right] \tag{12}$$
$$+G_k + G_b - \rho_f \epsilon_f - Y_M + S_k,$$

$$\frac{\partial}{\partial t}(\rho_f \epsilon_f) + \frac{\partial}{\partial x_j}(\rho_f \epsilon_f \boldsymbol{u}_f) = \frac{\partial}{\partial x_j}\left[\left(\mu_f + \frac{\mu_t}{\sigma_\epsilon}\right)\frac{\partial \epsilon_f}{\partial x_j}\right] \tag{13}$$
$$+\rho_f C_1 S \epsilon - \rho_f C_2 \frac{\epsilon^2}{\kappa + \sqrt{\nu \epsilon}} + C_{1\epsilon}\frac{\epsilon}{\kappa} C_{3\epsilon} G_b + S_\epsilon,$$

where $C_1 = \max\left[0.43; \frac{\eta}{\eta+5}\right]$, $\eta = S\frac{\kappa}{\epsilon}$, $S = \sqrt{2S_{ij}S_{ij}}$, μ_t is the turbulent viscosity, G_k represents the generation of turbulent kinetic energy due to the mean velocity gradient, G_b is the generation of turbulent kinetic energy due to buoyancy, Y_M represents the contribution of fluctuation, C_2 and $C_{1\epsilon}$ are constants, σ_κ and σ_ϵ are turbulent Prandtl numbers for κ and ϵ, respectively, and S_k and S_ϵ represent user-defined source terms. The "$\kappa - \epsilon$ Realizable" turbulence model used offers better performance (Ansys, 2013).

Lagrangian reference for particle trajectory, spherically solid particles, homogeneous particulate flow (particles of the same shape, dimensions, and properties), perfectly elastic collisions without change of shape or coalescence due to collision interactions, and neglected rotational motion about the center of mass are considered in the modeling of particulate flow.

According to Newton's Second Law, the ordinary differential equations governing the motion of the discrete phase are represented by Eqs. 14 and 15 (Ansys, 2013).

$$m\frac{\partial \boldsymbol{u}_p}{\partial t} = \boldsymbol{F}_d + \boldsymbol{F}_g + \boldsymbol{F}_{DEM}, \tag{14}$$

$$m\frac{\partial x_p}{\partial t} = \boldsymbol{u}_p, \tag{15}$$

where $\boldsymbol{u}_p$ is the particle velocity vector, $\boldsymbol{x}_p$ represents the particle position, $\boldsymbol{F}_d$ the drag force, $\boldsymbol{F}_g$ the gravity force and $\boldsymbol{F}_{DEM}$ the collision forces considered by the Discrete Element Method – DEM model (Cundall and Strack, 1979).

The main particle-fluid interaction force is the drag force $\boldsymbol{F}_d$, defined by Eq. 16, for a spherical particle of density ρ_p, diameter D_f and velocity $\boldsymbol{u}_p$ (Hryb *et al.*, 2009). C_d represents the particle drag coefficient defined by Eq. 17, where a_1, a_2 and a_3 are constants that apply over several ranges of the particle Reynolds number Re_p given by Morsi and Alexander (1972). The influence of the drag force can be quantified by the particle Reynolds number Re_p, which relates the inertial and viscous forces of the fluid acting on the particle, expressed by Eq. 18

Table 2. Dimensionless parameters.

Parameter	Symbol	Case 1	Case 2
Reynolds number	Re	126,771	633,857
Particle Reynolds number	Re_p	446.04	3440.64
Volumetric fractions of fluid	ε_f	0.999887	0.999887
Volumetric fractions of particles	ε_p	0.000113	0.000113
Stokes number	St	0.69	3.44

(Ansys, 2013; Hryb *et al.*, 2009).

$$\boldsymbol{F}_d = \frac{3}{4}\frac{\rho_f}{D_p} C_d (\boldsymbol{u}_f - \boldsymbol{u}_p)|\boldsymbol{u}_f - \boldsymbol{u}_p|, \tag{16}$$

$$C_d = a_1 + \frac{a_2}{Re_p} + \frac{3}{Re_p^2}, \tag{17}$$

$$Re_p = \frac{\rho_f D_p |\boldsymbol{u}_f - \boldsymbol{u}_p|}{\mu_f}, \tag{18}$$

the particle Reynolds number classifies the flow regime in which the particle is inserted, determining the appropriate drag force analysis.

The gravitational force $\boldsymbol{F}_g$ is defined by Eq. 19.

$$\boldsymbol{F}_g = \frac{\rho_p - \rho_f}{\rho_p}\boldsymbol{g}. \tag{19}$$

Collision forces are considered using the DEM model by the term $\boldsymbol{F}_{DEM}$. As defined in Eq. 20, these forces can be divided into a repulsive force due to the deformation of the particle $\boldsymbol{F}_n$, based on the stiffness modulus of the material, and a tangential frictional force $\boldsymbol{F}_t$, based on the Coulomb model of friction, which mainly depends on the relative velocity between the particle and fluid (Barbosa *et al.*, 2015).

$$\boldsymbol{F}_{DEM} = \boldsymbol{F}_n + \boldsymbol{F}_t. \tag{20}$$

In defining the mathematical model, boundary conditions are necessary and are the expressed, by using Fig. 3, as follows:

a) Input – the continuous phase input velocity was 1 and 5 m/s, according to Table 1. The particles are transported by the continuous phase and have the same continuous phase input velocity;
b) Output – a pressure level of 0 Pa was adopted;
c) Wall – stationary wall with non-slip and impenetrability conditions is valid.

The dimensionless parameters of the two cases are shown in Table 2.

D. Numerical model

The analysis of calcite precipitation on the inner wall of the horizontal well was numerically performed using the software Ansys Fluent®. An Intel® Core ™ i3, 3 GB RAM computer is used for the simulations.

The solution scheme of the equations was pressure-based. For pressure-velocity coupling the Phase Coupled SIMPLE (PC-SIMPLE) algorithm was employed. To evaluate the gradients of conserved properties, the Least Squares Cell-Based method was applied. The pressure interpolation scheme was First-Order. For the turbulent kinetic energy and turbulent dissipation rate, the scheme used was the First Order Upwind. For the transient formulation, the First Order Implicit procedure was adopted.

With the purpose of to get better results near the wall, Enhanced Wall Treatment was applied. This approach represents the near-wall flow using two layers with more sophisticated wall functions.

Table 3. DDPM-DEM parameters adopted.

Parameter	Model or value
Normal collision forces	Spring-dashpot collision model
Tangential collision forces	Friction collision model
Particle-particle coefficient of restitution	0.9
Particle-surface coefficient of restitution	0.5
Particle stiffness constant, N/m	100
Static friction coefficient	0.5
Sliding friction coefficient	0.2
Sliding velocity, m/s	1.0

Table 4. Number of elements of each mesh tested and computational effort.

Mesh number	Number of elements	Computational time to reach 20 seconds, hours
Mesh 1	61,824	1.22
Mesh 2	139,584	1.46
Mesh 3	387,158	2.11
Mesh 4	612,165	3.26

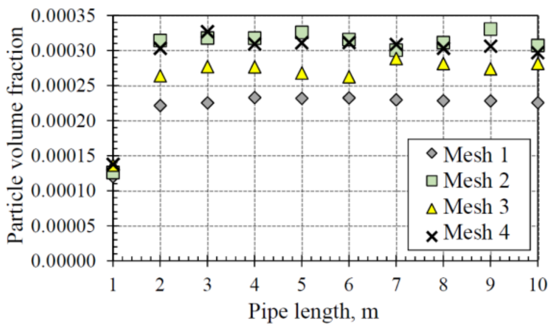

Figure 4. Comparisons of particle volume fraction along the pipeline in 20 seconds obtained with four levels of refinement.

The time step, Δt, for the particles was 0.01 s and for the continuous phase was 0.001 s.

In this paper, the use of DEM combined with the DDPM is essential to incorporate the effects of particle collisions. This approach represents the possible formation of particle packing. The collision forces are determined by the deformation, which is measured by small overlaps of the objects at the contacts (Ansys, 2013). The DDPM-DEM parameters used are detailed in Table 3.

The mesh test using tetrahedral elements was performed to evaluate the independence of the results from the level of refinement according to the details in Table 4. The DEM method was not used in this test. Figure 4 shows the discrete phase volumetric fraction, defined by Eq. 3, along the pipe in 20 seconds of flow. The continuous phase velocity is 1 m/s and the particles are injected with the same continuous phase velocity. Table 4 also presents the computational effort required to flow up to 20 seconds for each mesh. Since meshes 2 and 4 show good agreement on the discrete phase volumetric fraction representation (Fig. 4), with Mesh 2 being much less refined (139,584 elements as observed in Fig. 5) and requiring half the computational time (Table 3), was the mesh chosen with minimum orthogonal quality of approximately 0.83 and maximum aspect ratio of approximately 4.27.

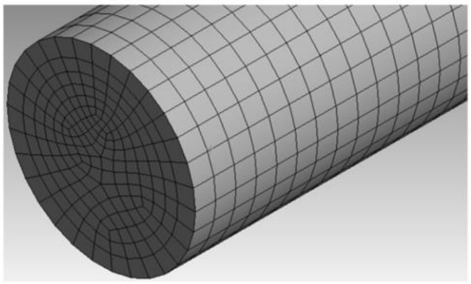

Figure 5. Partial view of adopted mesh consisting of 139,584 tetrahedral elements.

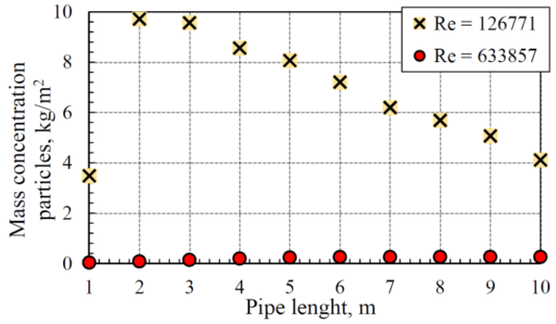

Figure 6. Particle deposition along the 10-m long pipeline in 20 seconds.

III. RESULTS AND DISCUSSIONS

To facilitate the presentation of the results, the pipe of 10 m length was divided into 10 equal parts. In each segment, average properties were calculated at the inner surface area, which are represented by points in the following figures.

A. Influence of injection flow rate

Figure 6 shows the particle deposition by the area of each segment along the pipe for two Reynolds numbers in the turbulent regime.

For $Re = 126{,}771$, with velocity equal to 1 m/s, there was a large accumulation of particles 10 kg/m^2 in the first 3 m of the pipe. From this distance, the deposition decreases almost linearly, reaching 4 kg/m^2 in the final interval. These phenomena occur due to the large influence of gravitational force on the particles and due to the relatively low velocity. For the case with $Re = 633{,}857$ (velocity 5 m/s), the particle deposition rate is practically negligible throughout the inner wall pipeline. It is justified because the higher velocity at this condition reduces gravitational effects on the particles compared with inertial effects.

Figure 7 represents the particle volume fraction, defined by Eq. 3, deposited along the wall pipe is insignificant in both situations, 0.02% and 0.004%, respectively, and as a consequence almost all particles reach the outlet plane. Greater influence of gravitational force can be observed when the inertia is comparatively lower, which results in a larger particle volume fraction throughout the pipeline. Both cases show a small increase in the particle volume fraction in the initial 3 m length, after that is approximately constant. This behavior is due to the flow dynamics that have the capacity to deposit particles that are flowing and to remove the deposited particles carrying them with continuous phase flow.

Table 5. Pressure variation in the pipeline for fluid flow with and without particles.

Re	Pressure variation	
	Without particles, Pa	With particles, Pa
126,771	708.51	722.20
633,875	12,850.19	12,873.32

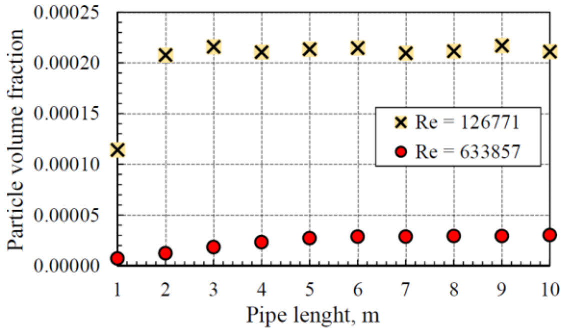

Figure 7. Particle volumetric fraction along the pipeline in 20 seconds.

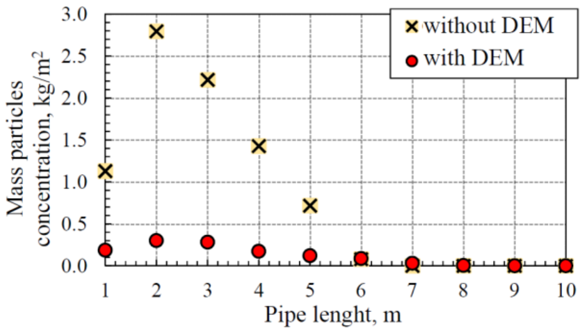

Figure 8. Particle deposition along the pipe in 7 seconds with ("o" symbol) and without ("x" symbol) the DEM method.

The influence of particles on the pressure drop simulating two cases is summarized in Table 5.

The presence of particles increases the pressure drop, 2% for $Re = 126{,}771$ and 0.2% for $Re = 633{,}875$, which is greater for lower Reynolds number. Since the Stokes number is less than the critical value, $St < St_c$, for both cases (Table 2), the pressure drop is not pronounced because the particles do not strongly influence the flow.

B. Influence of DEM method

The Discrete Element Method – DEM method can represent the collisions between particles, which would make the obtained results closer to what occurs in a real environment. However, its use leads to a sharp increase in computational effort, making difficult to perform tests in complex geometries.

Therefore, the flow in our research was analyzed only up to 7 seconds, which means 97 h at all, almost 8 times longer than modeling without DEM (Table 6). It represents approximately one-third of particle residence time. Figure 8 shows the particle deposition and Fig. 9 the particle volumetric fraction for cases with and without the use of DEM method.

In the case without the DEM approach, the gravitational effects are predominant (Fig. 8), indicating a significant deposition at the beginning of the pipe and a sharp reduction in the deposition from approximately 2 meters from the pipe inlet. Because other forces are incorporated in the DEM approach, such as collisional force, the gravitational force is not more dominant and the mass particle deposition by a square inner surface of the pipe is insignificant.

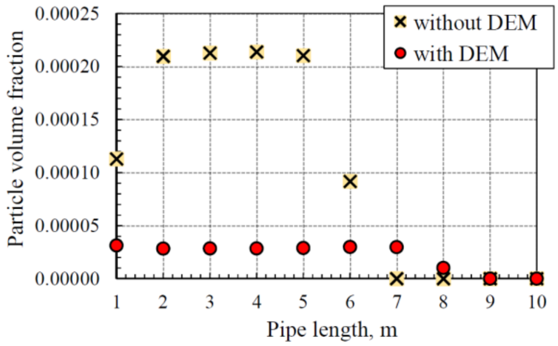

Figure 9. Particles volumetric fraction along the pipe in 7 seconds in cases with and without the DEM method.

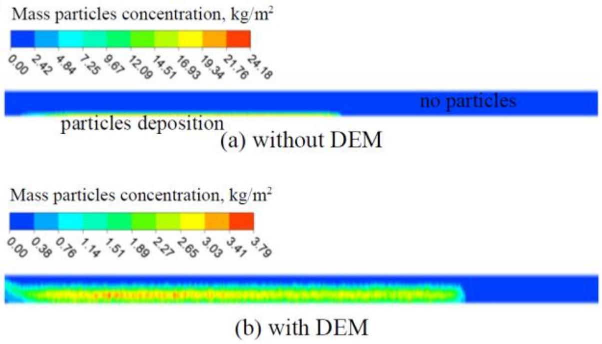

Figure 10. Mass particle concentration fields along the pipe in 7 seconds. The field has different scales. To improve visualization, the vertical length has been increased.

The analysis of particle volume fraction for two scenarios in Fig. 9 shows that not incorporating DEM model results in a larger number of particles deposited in the first half of pipe, and practically no particles in the last three meters. The DEM modeling has a low and nearly constant particle value. These results show the great influence of the gravitational force on the case without DEM approach. While in the case with the DEM method, the particles are carried by the flow since as commented, the gravitational force is not more the only acting force.

The particles (of calcium carbonate) mass concentration field throughout the pipe, within 7 seconds of flow, obtained without and with the DEM method is shown in Fig. 10. The particles are injected into the left face and their absence is identified by the blue color (in the online version).

In both cases, the particles are concentrated at the bottom of the pipe, characterizing the particle deposition process due to the gravitational force. This behavior is due to the large size of the injected particles. The case without the DEM method has a higher particle concentration (maximum 24.18 kg/m^2, Fig. 10a) in a more limited space than the case with the DEM method (maximum 3.79 kg/m^2, Fig. 10b). This phenomenon may have occurred due to the high influence of the gravitational

Table 6. Computational effort required to flow reach 7 seconds.

Approach Computational	time, hours
Without DEM	12
With DEM	97

force and the presence of collision forces on the particles in the case with the DEM method.

Table 6 presents the computational effort required for the flow to reach 7 seconds for each case. When using the DEM method, it takes approximately 85 additional hours for the flow to reach 7 seconds. Due to this feature, applying the method to more complex geometries can be impracticable.

IV. CONCLUSIONS

A phenomenological methodology based on CFD tools to analyze a transient, turbulent, three-dimensional and biphasic flow of deposition of particles, representing $CaCO_3$, on the inner wall of a horizontal pipe and in well conditions was presented in this study. The following conclusions stand out:

a) The problem is complex in terms of computational capacity requirement, difficulty in choosing appropriate simulation parameters and scarcity of results in the literature for comparison;
b) The particle deposition by square inner wall is higher for lower injection velocity or Reynolds numbers;
c) The presence of particles has little influence on the flow because the Stokes number is small ($St < St_c$) for the analyzed cases;
d) There is a strong influence of gravitational force for cases without DEM approach because no other forces are considered in the modeling;
e) There was a better representation of the behavior of particles with DEM approach, however, its use demands a high computational cost.

In future work, it is suggested to reduce particle size to better represent $CaCO^3$ scaling and to solve the problem using the Euler-Euler approach.

ACKNOWLEDGEMENTS

The authors would like to thank Petrobras SA to financially support this research. Also, Professor Oldrich Joel Romero would like to thank FAPES – Espírito Santo Research and Innovation Support Foundation for the financial support through “Edital FAPES 18/2018 – BPC”.

REFERENCES

Al Nasser, W.N., Shaikh, A., Morriss, C., Hounslow, M.J. and Salman, A.D. (2008) Determining kinetics of calcium carbonate precipitation by inline technique. *Chemical Engineering Science*. **63**, 1381-1389.

Ansys Inc. (2013*) ANSYS Fluent Theory Guide*. Release 15.0.

Barbosa, M.V., De Lai, F.C., Franco, A.T. and Junqueira, S.L.M. (2015) Parametric analysis of particulate flow for fluid loss control applied to sealing fractured channels. 23rd *ABCM International Congress of Mechanical Engineering*. Rio de Janeiro, Brazil.

Chen, Y. and Chung, J.N. (1995) The linear stability of an oscillatory two-phase channel flow in the limit of small Stokes numbers. *Physics of Fluids*, **7**, 1510–1512.

Cosmo, R.P, Pereira, F.A.R., Ribeiro, D.C., Barros, W.Q. and Martins, A.L. (2019) Estimating CO_2 degassing effect on $CaCO_3$ precipitation under oil well conditions. *Journal of Petroleum Science and Engineering*. **181**, 1-8.

Cowan, J.C. and Weintritt, D.J. (1976) *Water-formed scale deposits*. Gulf Publishing Company. Houston Texas.

Crowe, C.T., Schwarzkopf, J.D., Sommerfield, M. and Tsuji, Y. (2011) *Multiphase Flows with Droplets and Particles.* CRC Press.

Cundall, P.A. and Strack, O.D.L. (1979) A discrete numerical model for granular assemblies. *Geotechnique*. **29**, 47–65.

Gondret, P., Lance, M. and Petit, L. (2002) Bouncing motion of spherical particles in fluids. *Physics of fluids*. **14**, 643-652.

Hadinoto, K. and Chew, J.W. (2010) Modeling fluid–particle interaction in dilute-phase turbulent liquid–particle flow simulation. *Particuology*. **8**, 150-160.

Hrenya, C.M. and Sinclair, J.L. (1997) Effects of particle-phase turbulence in gas-solid flows. *AIChE Journal*. **43**, 853–869.

Hryb, D., Cardozo, M., Ferro, S., and Goldschmit, M. (2009) Particle transport in turbulent flow using both Lagrangian and Eulerian formulations. *International Communications in Heat and Mass Transfer*. **36**, 451-457.

Morsi, S.A. and Alexander, A.J. (1972) An investigation of particle trajectories in two-phase flow systems. *Journal of Fluid Mechanics*. **55**, 193–208.

Ojaniemi, U., Riihimäki, M., Manninen, M. and Pättikangas, T. (2012) Wall function model for particulate fouling applying XDLVO theory. *Chemical Engineering Science*. **84**, 57-69.

Popoff, B. and Braun, M. (2007) A Lagrangian Approach to Dense Particulate Flows. *International Conference on Multiphase Flow*. Leipzig, Germany.

Vazirian, M.M., Charpentier, T.V.J., Penna, M.O. and Neville A. (2016) Surface inorganic scale formation in oil and gas industry: As adhesion and deposition processes. *Journal of Petroleum Science and Engineering*. **137**, 22-32.

Received: October 6, 2019
Sent to Subject Editor: October 10. 2019
Accepted: January 13, 2021
Recommended by Subject Editor Walter Tuckart